Available online at www.sciencedirect.com
ScienceDirect
Trans. Nonferrous Met. Soc. China 35(2025) 2201−2216
Transactions of Nonferrous Metals Society of China
www.tnmsc.cn

Effect of hot-rolling deformation on grain, texture and formability of Al−Mg−Si−Zn alloy sheets

Kai-xin CHEN[1,2,3], Li-zhen YAN[1,2,3], Yong-an ZHANG[1,2,3], Xi-wu LI[1,2,3], Zhi-hui LI[1,3], Hong-wei YAN[1,2,3], Lei CHEN[4], Guan-jun GAO[1,2], Bai-qing XIONG[1,3]

1. State Key Laboratory of Nonferrous Metals and Processes, China GRINM Group Co., Ltd., Beijing 100088, China;
2. GRIMAT Engineering Institute Co., Ltd., Beijing 101407, China;
3. Research Institute for Nonferrous Metals, Beijing 100088, China;
4. Northeast Light Alloy Co., Ltd., Harbin 150060, China

Received 31 October 2023; accepted 19 July 2024

Abstract: The effects of Al(Fe,Mn)Si particles controlled by different hot-rolling deformations on the microstructure evolution, texture evolution, and formabilities of Al−Mg−Si−Zn alloy were systematically investigated using OM, SEM, TEM, XRD, and tensile tests. The results indicate that Al(Fe,Mn)Si particles with different size and number distribution characteristics can be obtained by adjusting the hot-rolling deformation degree (59%, 74% and 87%), and these differences in particle distribution are the main factors affecting the recrystallization nucleation and grain growth during solution treatment. After T4P treatment, the grain orientations in the Al−Mg−Si−Zn alloy sheets with 59% and 74% hot-rolling deformation tend to be randomly distributed. In comparison, the sheet with 87% hot-rolling deformation consists of R{124}⟨211⟩, Cube_{ND} {100}⟨013⟩, Copper{112}⟨111⟩ and Brass{011}⟨211⟩ texture components. The medium size and number of Al(Fe,Mn)Si particles obtained at 74% hot-rolling deformation cause fine grains and randomly distributed texture, which significantly improves the formability of Al−Mg−Si−Zn alloy.

Key words: Al−Mg−Si−Zn alloy; hot-rolling deformation; Al(Fe,Mn)Si particles; grain; texture; formability

1 Introduction

Recently, in response to the demand for environmental protection and the growth of new energy vehicles, aluminum alloys have been increasingly used in the automotive industry due to their low density [1−3]. Among those aluminum alloys, the heat-treatable Al−Mg−Si alloys are extensively used for automotive panels owing to their excellent baking-hardening property and formability [4−7]. The limit drawing ratio (LDR) can more accurately assess the formability of alloy sheets [8]. It is shown that the higher the limit drawing ratio, the better the formability. LEU [9] stated that the LDR value is primarily influenced by the average plastic strain ratio (r) and the strain hardening index (n). The LDR value is usually expressed as follows:

$$\text{LDR}=\sqrt{\exp\left[\left(2f\exp(-n)\right)\sqrt{\frac{1+r}{2}}\right]+\exp\left[2n\sqrt{\frac{1+r}{2}}\right]-1} \tag{1}$$

where f is the drawing efficiency. Many studies have shown that the formability and mechanical property anisotropy of alloys are influenced by the

Corresponding author: Li-zhen YAN, Tel: +86-10-60662659, E-mail: yanlizhen@grinm.com;
Yong-an ZHANG, Tel: +86-10-60662652, E-mail: zhangyongan@grinm.com
https://doi.org/10.1016/S1003-6326(25)66809-9

composition of the textures and their intensities strongly. Two initial textures of γ-fibers ($\{111\}\langle uvw\rangle$) and random orientation are favorable to improving formability [10−12]. Furthermore, the texture is strongly influenced by chemical elements and processing parameters [5,13,14].

The typical manufacturing processes for producing Al−Mg−Si alloy sheets include casting, homogenization, hot-rolling, intermediate annealing, cold-rolling, solution treatment, and pre-aging. As the first step of sheet processing, hot-rolling has an essential genetic effect on the subsequent microstructure and texture evolution. Moreover, the hot-rolling process is complex and involves various influencing factors, but most research on hot-rolling has focused on the effect of hot-rolling temperature on the microstructure and texture of Al−Mg−Si alloy sheets. It has been shown that Al−5Mg−0.8Mn alloys undergo dynamic recrystallization during hot deformation at 400−500 °C, while their subgrain diameter is smaller than that of commercial Al alloy as a result of the increased density of particles [15]. LI et al [16] found a similar texture gradient in Al−Mg−Si alloy. For Al−Mg−Si alloy, the Cube texture in the hot-rolled sheet increases significantly at higher hot-rolling exit temperatures, which is easily retained and inherited to T4P-treated microstructure. Moreover, the presence of a large quantity of Mg_2Si particles hinders the particle-simulated nucleation (PSN) effect and encourages the formation of cube texture during solution treatment [14]. Our previous study [17] found that the hot-rolling temperature affects the precipitation of Mg_2Si and Si particles in Al−Mg−Si alloy sheets, and the distribution of these precipitated particles improves the formability at an initial rolling temperature of 555 °C. Moreover, another study on the effect of Al(Fe,Mn)Si particles is still focused only on the compositional adjustment of the Al−Mg−Si alloys. For example, in Al−Mg−Si−Cu alloy, the effect of solid solution time on grain structure and texture becomes less significant with the increase of the concentration of Al(Fe,Mn)Si particles, indicating that Al(Fe,Mn)Si particles are beneficial to improving the stability of grain structure [18−20].

In summary, it can be found that most investigations on hot-rolling mainly focused on the influence of the hot-rolling process for hot-rolled microstructure and texture. The microstructure and texture evolution of Al−Mg−Si−Zn alloy sheets after subsequent processing lacks systematic analysis. There is less report on the hot-rolling deformation of Al−Mg−Si−Zn alloy sheets, and in particular, controlling the Al(Fe,Mn)Si particles by mechanical processing has yet to be found. However, Al(Fe,Mn)Si particles and the microstructure and texture of finished sheets are significantly affected by the hot-rolling process. Therefore, this work aimed to modulate the size and distribution of insoluble Al(Fe,Mn)Si particles in the Al−Mg−Si−Zn alloy by varying hot-rolling deformation, and their influence on the evolution of recrystallization microstructure and texture during subsequent processing was also revealed. Further, relevant relationship among particles, grain, texture, and formability was investigated carefully, and the mechanisms were discussed systematically. It provided a guidance for optimizing the hot rolling process to improve the formability of the Al−Mg−Si−Zn alloy sheet in automotive industry.

2 Experimental

The as-received material was a homogenized Al−Mg−Si−Zn alloy with a thickness of 40 mm and a chemical composition of Al−0.8Mg−1.02Si−0.6Zn−0.18Cu−0.12Fe−0.08Mn (wt.%). The sheets were hot-rolled to a thickness of (5.3±0.1) mm through rolling schemes A, B and C in Table 1, respectively. Through our preliminary study [17], it was necessary to establish the initial rolling temperature of the alloy at 555 °C and control the exit temperature to 210−230 °C. After cooling to room temperature, these sheets were cold-rolled to a thickness of 1.8 mm. Afterward, they were intermediately annealed at 450 °C for 1 h before undergoing another cold-rolling process to reach a final thickness of 0.95 mm. Then, the sheets were solution treated at 560 °C for 5 min, followed by water quenching. Finally, these sheets were

Table 1 Hot-rolling processes of Al−Mg−Si−Zn alloy sheets

Scheme	Total hot-rolling deformation degree/%	Reduction per pass/%
A	59	14−30
B	74	
C	87	

pre-aged at a cooling rate of 4 °C/h in the temperature range of 90−60 °C (T4P treatment).

The Zeiss Axiovert Imager A2m optical microscope (OM) was used to observe the microstructure of the alloy sheet on a plane parallel to the transverse direction (RD). The samples were analyzed using a JSM−7001F scanning electron microscope (SEM) with X-ray energy dispersive spectrometer (EDS) to examine the coarse particle distribution. The electron backscatter diffraction (EBSD) was performed at a voltage of 20 kV and a scanning step size of 2.5 μm. The fine particle distribution was investigated using a Talos F200X G2 transmission electron microscope and a SUPRA 55 SEM. Transmission electron microscopy (TEM) samples were thinned on both sides by ion beam bombardment at −120 °C using a 695.0 PIPS II ion beam thinner. X-ray pole figure measurements were used to characterize textures at a quarter thickness of the sheets. Four incomplete polar maps with indices of (111), (200), (220), and (311) were obtained with Bruker D8 Discover X-ray diffractometer at 40 kV and 40 mA of Cu K_α radiation using the Schulz back-reflection method. The incomplete pole figures (l_{max}=16) were utilized to compute the orientation distribution functions (ODFs) via the series expansion method.

The mechanical properties of three T4P-treated alloy sheets were tested on the MTS−WD3100 at room temperature. The tensile tests of the sheets were performed at 0°, 45° and 90° with respect to the rolling direction according to EN ISO 6892-1 standard. The *r* value was calculated using a tensile strain of 10%, and the *n* value was determined in the 10%−20% strain range. At least three specimens in each direction were tested, and their average values were reported.

3 Results

3.1 Microstructure evolution

Figure 1 exhibits the hot-rolling microstructure of three alloy sheets. It can be seen that there are apparent differences in the grain morphology of different hot-rolling deformation degrees. Sheets A and B consist of elongated grains along the rolling direction, and the aspect ratio of grains decreases significantly with the increase of hot-rolling deformation degree. Sheet C is characterized by highly elongated bands along the rolling direction. With the increase of deformation degree, the grain structure of the hot-rolled sheet is gradually elongated, and the layer spacing of the grain structure is gradually reduced. Furthermore, there are some differences in the microstructure of the surface and middle layers. Compared with the middle layer, the layer spacing of the surface layer is more minor. The coarse particles distributed in these three alloy sheets are presented in Fig. 2. A large number of grayish-white particles display banded interrupted distribution along the grain boundaries, which are identified as Al(Fe,Mn)Si particles according to the energy spectrum analysis, as shown in Fig. 2(d). The size and number of coarse Al(Fe,Mn)Si particles distributed in the three sheets are significantly different, and their statistical

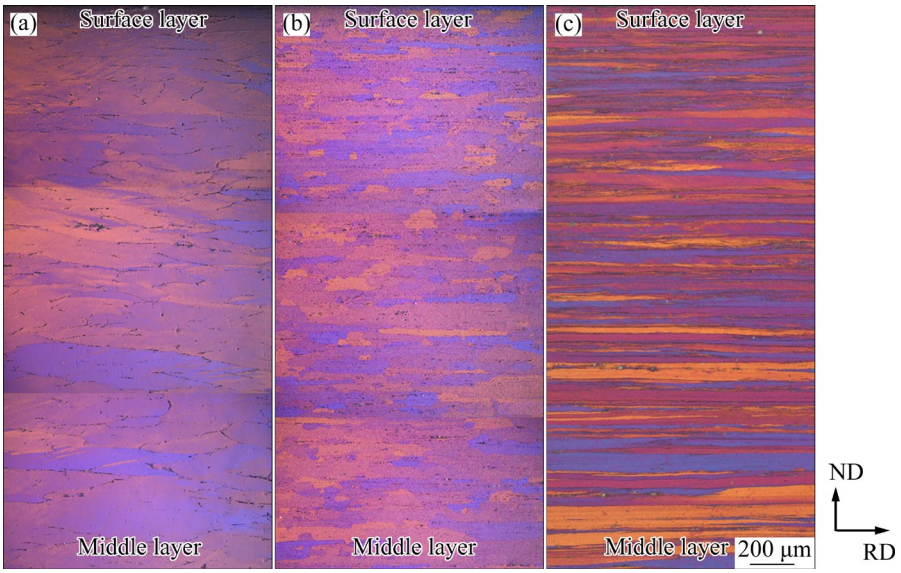

Fig. 1 Hot-rolled microstructures of alloy sheets: (a) Sheet A; (b) Sheet B; (c) Sheet C

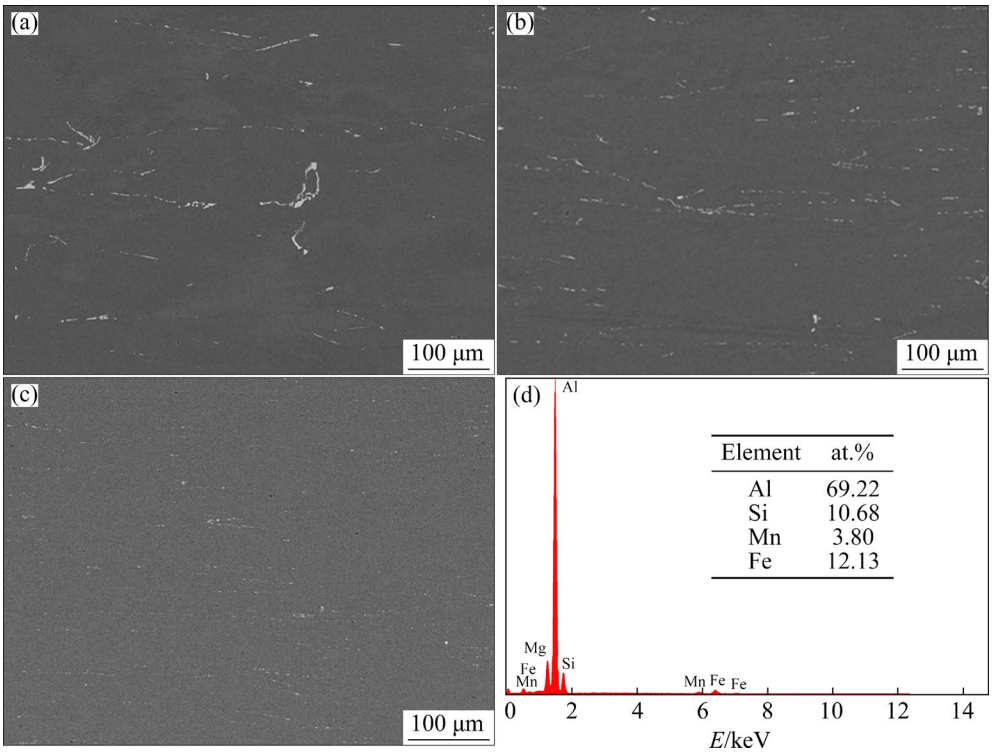

Fig. 2 SEM micrographs of hot-rolled alloy sheets: (a) Sheet A; (b) Sheet B; (c) Sheet C; (d) EDS spectrum of particle

results are given in Table 2. The number of Al(Fe,Mn)Si particles follows order of Sheet C > Sheet B > Sheet A, and the size of Al(Fe,Mn)Si particles follows the order of Sheet A > Sheet B > Sheet C. This may be due to the different deformation degrees during the hot-rolling process.

Table 2 Detailed statistical information of Al(Fe,Mn)Si particles in hot-rolled alloy sheets

Alloy sheet	Number density/mm^{-2}	Diameter/ μm	Area fraction/%
A	1.44×10^3	2.81	1.07
B	2.22×10^3	2.25	1.06
C	2.85×10^3	1.88	1.01

The hot-rolled alloy sheets are cold-rolled to a final thickness of 0.95 mm. The OM micrographs of the cold-rolled alloy sheets are shown in Fig. 3. The microstructures of Sheets B and C are very similar, and both are composed of elongated deformed grains. In comparison, the spacing between the surface and middle layers of Sheets B and C is the same. At the same time, a small amount of coarse elongated grains also exist in the middle layer of Sheet A. Among the three sheets, the grain structure of Sheet A is relatively coarse. During the following intermediate-annealing and cold-rolling, particle distribution is changed, and SEM micrographs of the particles in the cold-rolled alloy sheets are shown in Fig. 4. Due to the intermediate annealing treatment, black Mg_2Si particles with submicron size are also precipitated. During the following cold-rolling, the coarse Al(Fe,Mn)Si particles in the three sheets show a similar behavior and are further crushed, decreasing in average size and increasing in number. The average Al(Fe,Mn)Si particle sizes in Sheets A, B and C are 0.53, 0.40 and 0.37 μm, respectively.

Figure 5 shows the distribution of fine particles in the cold-rolled sheet. According to EDS analysis in Figs. 5(d−f), three kinds of particles can be identified. The irregular-shaped or spherical particles are identified as Mg_2Si, and the rod-like or irregular-shaped particles are identified as Si, partially similar in morphology for both particles. The fine rod-like or spherical particles are identified as Al(Fe,Mn)Si. The fine Al(Fe,Mn)Si particles are formed by crushing the coarse Al(Fe,Mn)Si particles during hot and cold rolling and precipitation of the previous homogenization process. As can be seen in Figs. 4 and 5, the sizes of Mg_2Si and Si particles in all three sheets are small, mostly below 1 μm, and their distributions are

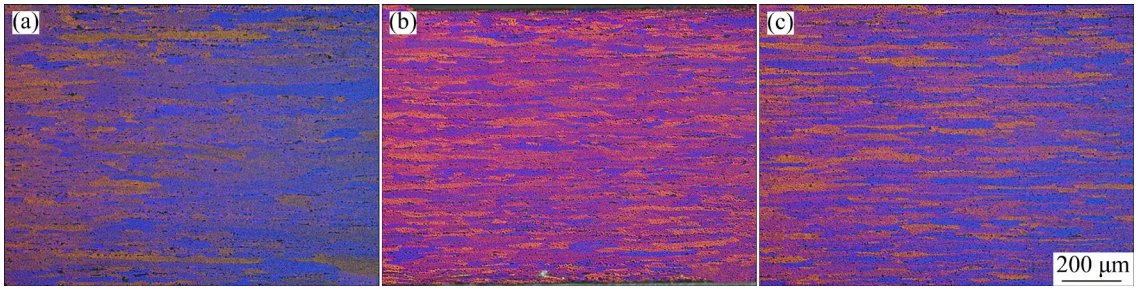

Fig. 3 Cold-rolled microstructures of alloy sheets: (a) Sheet A; (b) Sheet B; (c) Sheet C

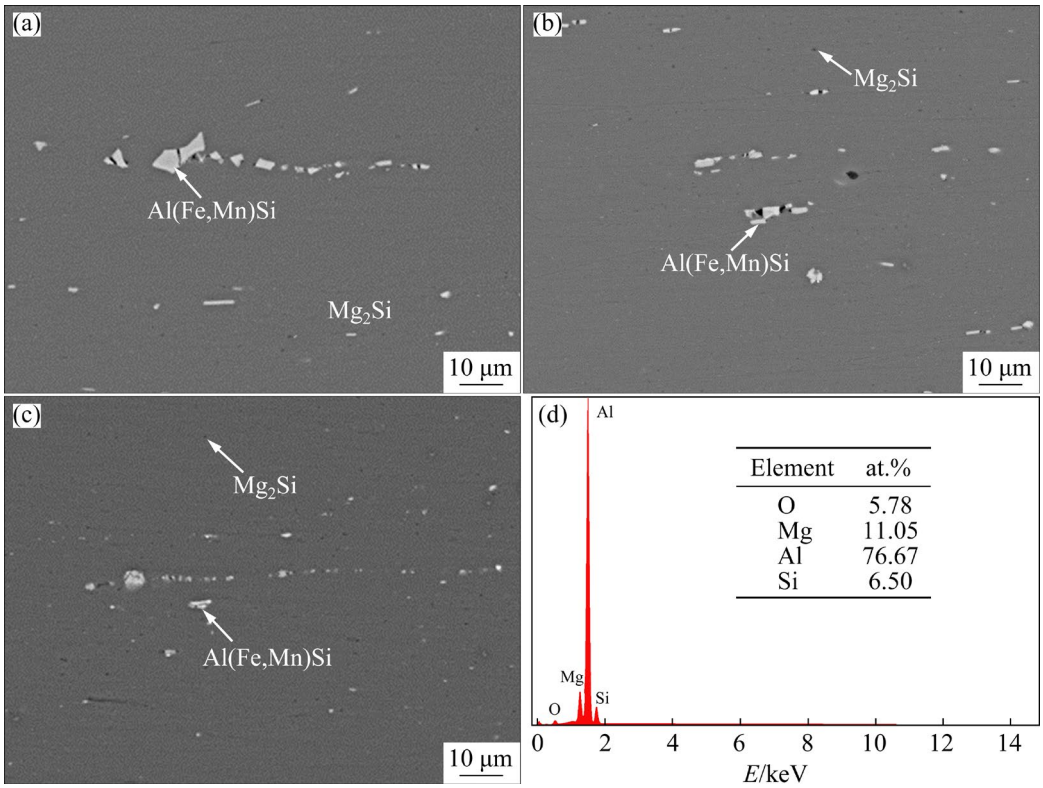

Fig. 4 SEM micrographs of cold-rolled alloy sheets: (a) Sheet A; (b) Sheet B; (c) Sheet C; (d) EDS spectrum of particle

similar, which may be related to the same hot rolling temperature and intermediate annealing treatment. Therefore, the effects of Mg_2Si and Si particles on the microstructure and texture evolution of the three sheets during the subsequent solution treatment, and on the properties of the T4P-treated sheets are identical. To avoid the excessive dislocations in the cold-rolled sheet masking the distribution information of the fine Al(Fe,Mn)Si particles, the TEM results of the T4P-state sheets are supplemented, as shown in Fig. 6. After T4P treatment, Mg_2Si and Si particles are completely dissolved back into the matrix, and only insoluble Al(Fe,Mn)Si particles are observed with the same distribution pattern as in the cold-rolled microstructure.

The statistical results of Al(Fe,Mn)Si particles distributed in the three sheets are shown in Fig. 7. It can be found that the number density of Al(Fe,Mn)Si particles below 0.2 μm increases gradually with the increase of hot rolling deformation degree. The size and number distribution patterns of Al(Fe,Mn)Si particles in the three cold-rolled sheets are basically the same as those in the hot-rolled sheets due to the same process of cold-rolling deformation. Based on the analysis, it can be concluded that the size and distribution of coarse Al(Fe,Mn)Si particles vary significantly due to the hot-rolling deformation. This, in turn, has a particular impact on the microstructure of the cold-rolled sheets and ultimately affects the recrystallization process during the solution treatment.

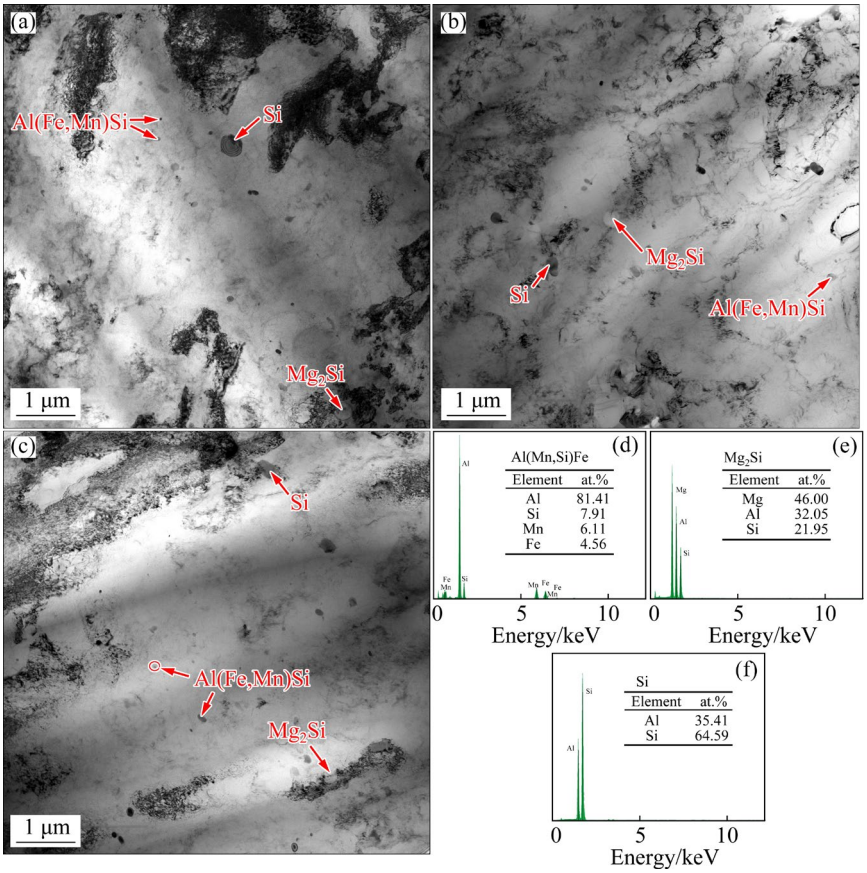

Fig. 5 TEM micrographs of cold-rolled alloy sheets: (a) Sheet A; (b) Sheet B; (c) Sheet C; (d−f) EDS spectra of particle

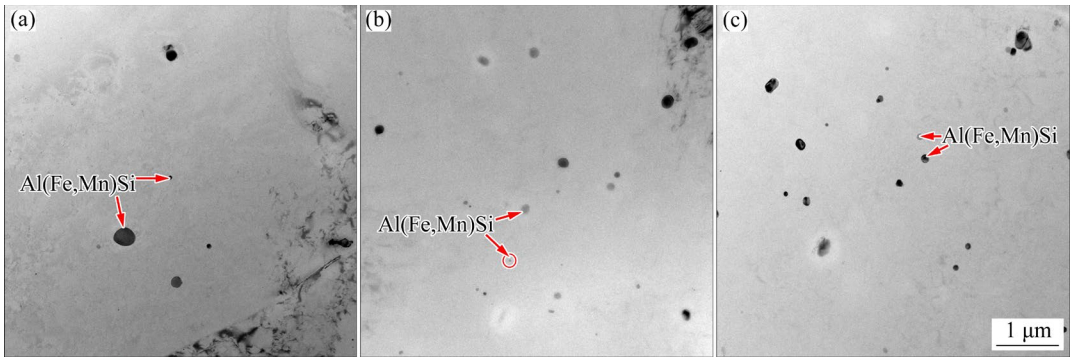

Fig. 6 TEM micrographs of T4P-treated alloy sheets: (a) Sheet A; (b) Sheet B; (c) Sheet C

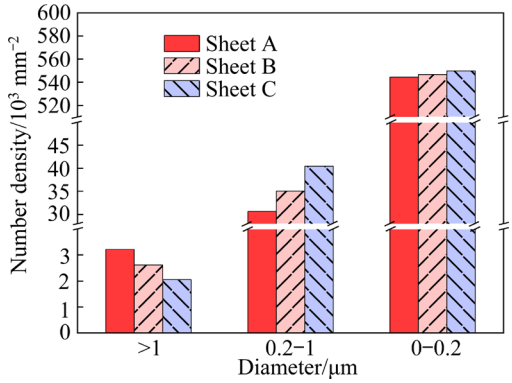

Fig. 7 Detailed statistical information of Al(Fe,Mn)Si particles in cold-rolled alloy sheets

After solution treatment, alloy sheets exhibit equiaxed grains, replacing the previously deformed grains, as shown in Fig. 8. Based on EBSD statistical calculations, it is determined that the average grain sizes for Sheets A, B, and C are 46.26, 38.26, and 48.28 μm, respectively. It can be found that the recrystallized grain structure of Sheet B is the most homogeneous, while there are recrystallized grains with sizes over 100 μm in Sheet A. It is possible that the variations in the final recrystallization microstructure among the three sheets can result in distinct formabilities.

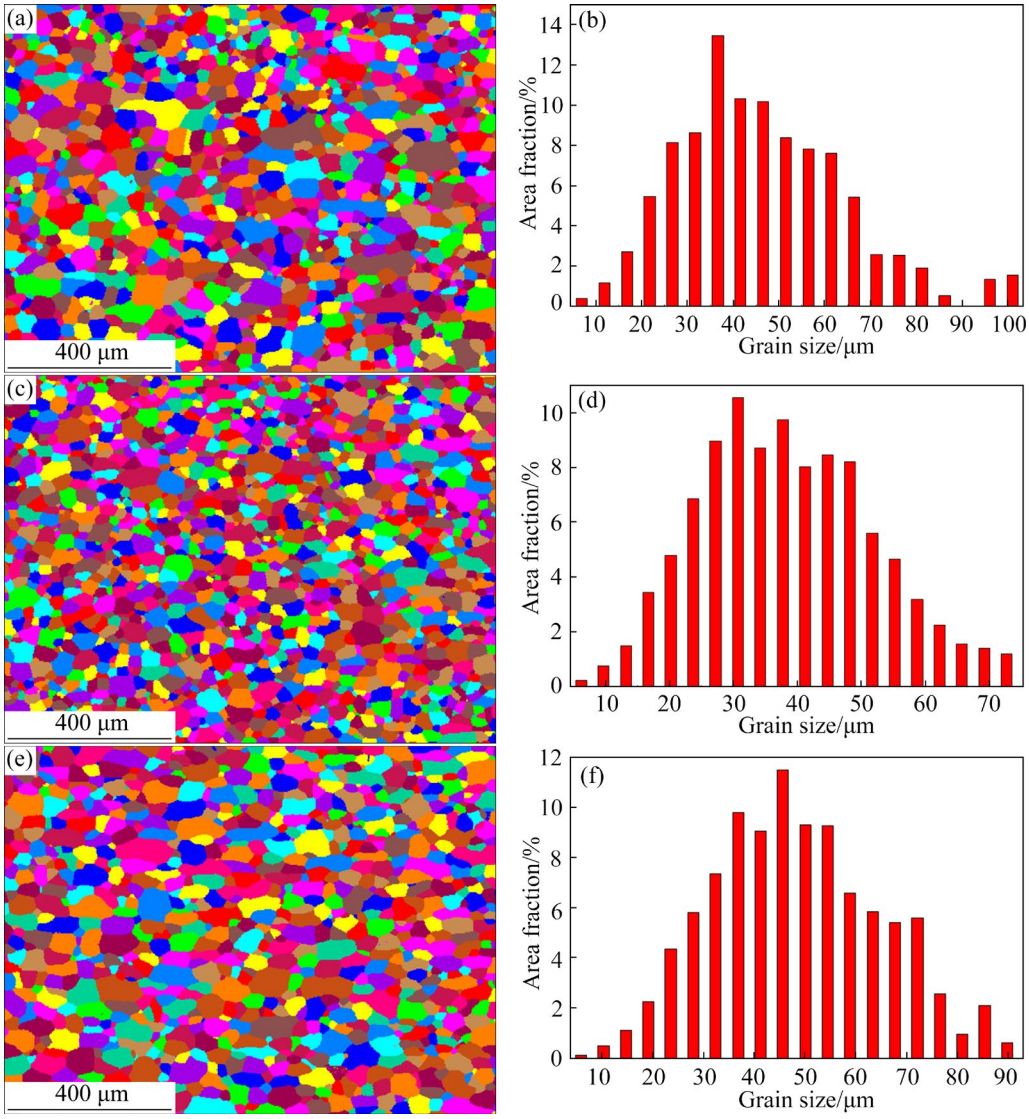

Fig. 8 EBSD maps of T4P-treated alloy sheets: (a) Grain microstructure of Sheet A; (b) Grain size distribution of Sheet A; (c) Grain microstructure of Sheet B; (d) Grain size distribution of Sheet B; (e) Grain microstructure of Sheet C; (f) Grain size distribution of Sheet C

3.2 Texture evolution

Figure 9 shows the ODFs of the alloy sheets after three hot-rolled processes. There are some sub-stable orientations in the sheets, which are more easily transformed in the subsequent processing. It can be observed that Sheet A is dominated by the sub-stable {013}⟨531⟩ orientation with an intensity of 4.04, while a small amount of S {123}⟨634⟩ and Copper {112}⟨111⟩ orientations with intensities of 2.27 and 2.10, respectively, are present. The main texture component of Sheets B and C is the β-fiber orientation (The spatial orientation is from the Copper orientation through the S orientation to the Brass {011}⟨211⟩ orientation [21,22]). In Sheet B, the deformation textures, Copper, S and Brass, are significantly increased with orientation intensities of 7.96, 8.34 and 6.38, respectively, and a minor amount of Goss {110}⟨001⟩ and {014}⟨100⟩ orientations with orientation intensities of 3.27 and 2.36 are also present. Sheet C consists mainly of the deformation textures Copper, S and Brass with orientation intensities of 6.96, 7.20 and 8.46, respectively, forming a recrystallized Cube {100}⟨001⟩ texture with an orientation intensity of 2.48. This reveals that the larger the deformation degree, the easier the formation of Brass and recrystallized textures at the same hot-rolling temperature. It can be noticed that different hot-rolling deformations significantly affect the type and intensities of the textures in the

hot-rolled sheets.

Figure 10 shows the ODFs of cold-rolled alloy sheets, and Fig. 11 shows statistical results of texture distribution. Obviously, after cold-rolling, all three sheets exhibit β-fiber, and their β-orientation intensities tend to be similar, but the position of β-fibers slightly deviates from the theoretical position. In addition, some of the recrystallization textures formed during the intermediate annealing treatment are not entirely transformed into deformation textures during the subsequent cold-rolling of the sheets. Because the cold-rolling deformation degree after intermediate annealing is only 47%, the recrystallized textures, Goss, $Cube_{RD}$ and Cube, formed during intermediate annealing are retained after cold-rolling. In Sheet A, the $Cube_{RD}$ $\{013\}\langle100\rangle$ (Cube orientation rotating around the rolling direction) and Goss texture are present with orientation intensities of 2.43 and 2.61, respectively. Sheet B also has $Cube_{RD}$ and Goss textures with orientation intensities of 2.35 and 2.12, which is slightly different from Sheet A. In Sheet C, Cube and Goss textures are observed with orientation intensities of 4.72 and 2.76, respectively. It can be seen that there are only some differences in the

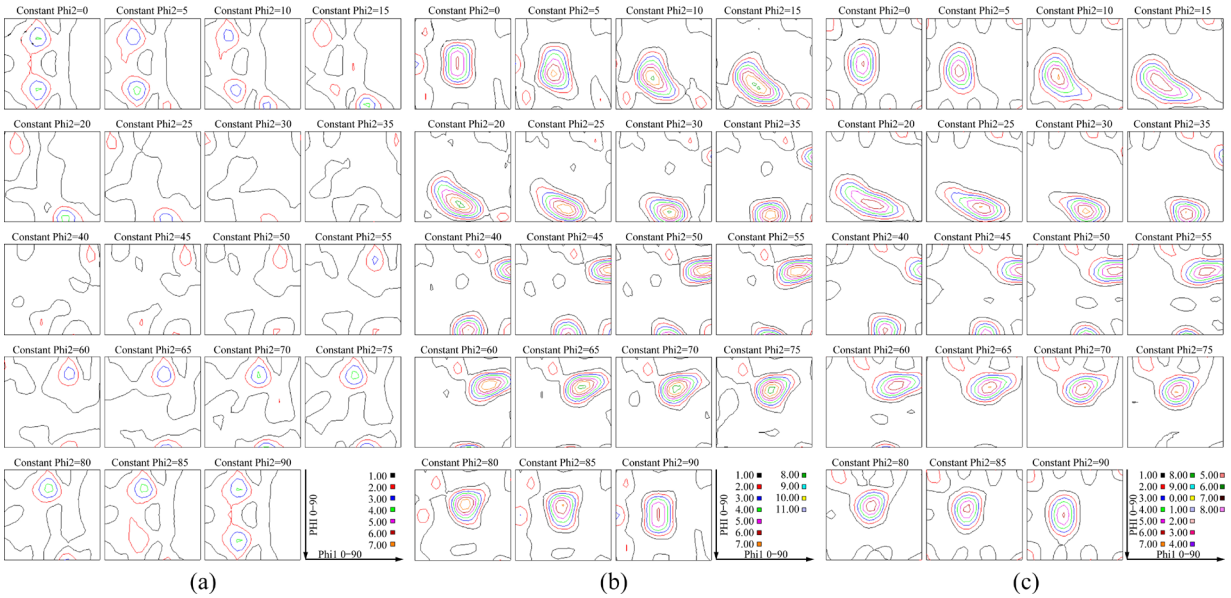

Fig. 9 ODFs of hot-rolled alloy sheets: (a) Sheet A; (b) Sheet B; (c) Sheet C

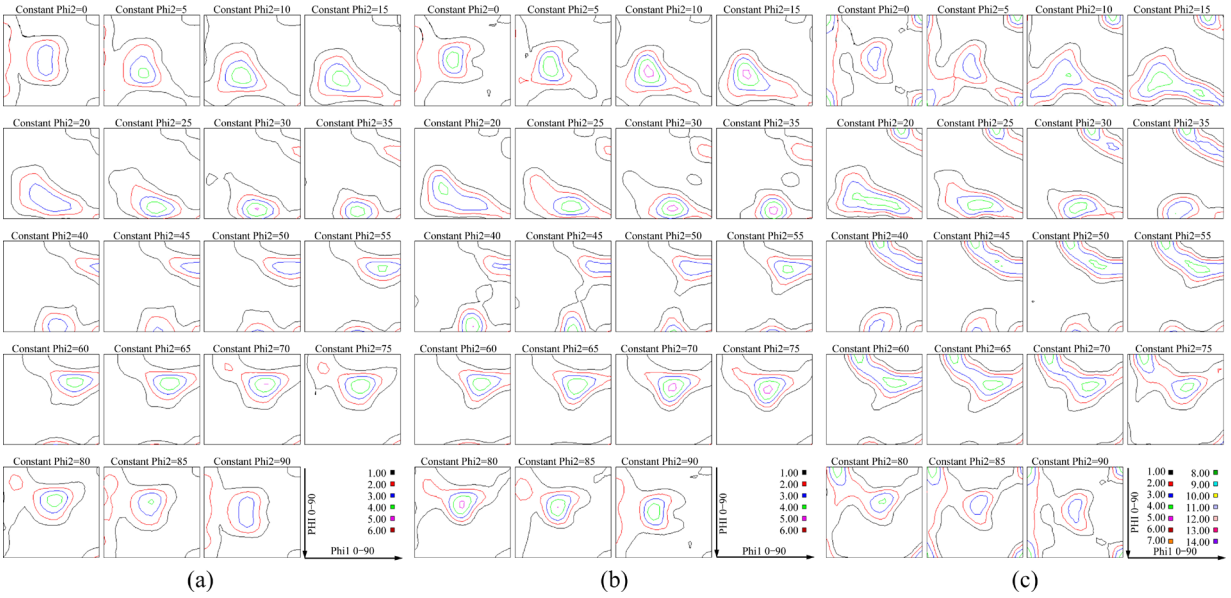

Fig. 10 ODFs of cold-rolled alloy sheets: (a) Sheet A; (b) Sheet B; (c) Sheet C

recrystallization textures in the three alloy sheets. Therefore, the slight difference in the texture distribution of the cold-rolled sheets is only a minimal part of the variation in the final recrystallization texture.

Figure 12 shows the ODFs of T4P-treated alloy sheets. After solution treatment, the grain orientation of Sheets A and B shows a random distribution. However, Sheet C is dominated by the recrystallization texture R {124}⟨211⟩, $Cube_{ND}$ {100}⟨013⟩ (Cube orientation rotating around the normal direction) and $Cube_{RD}$ with orientation

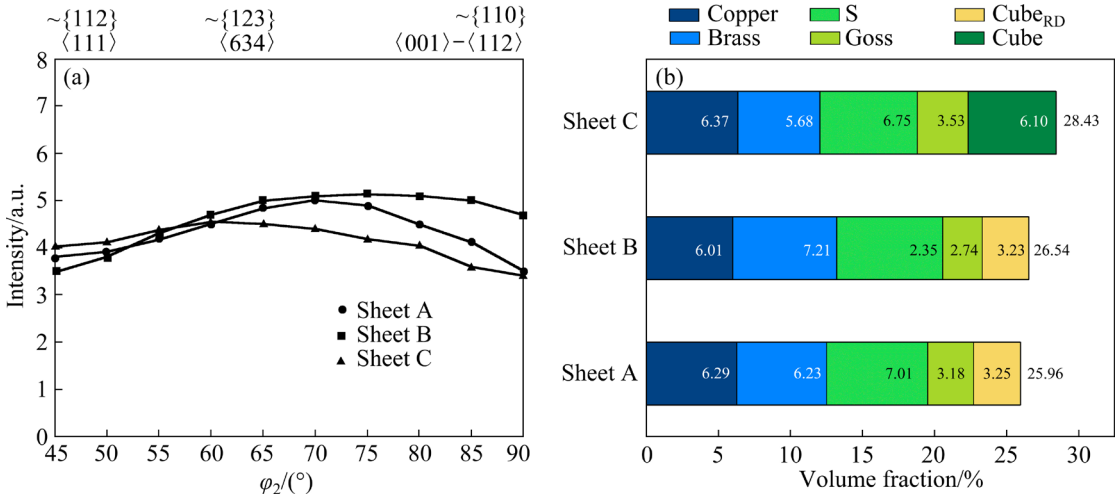

Fig. 11 Texture distribution in cold-rolled alloy sheets: (a) Orientation intensity along β-fiber distribution; (b) Volume fractions

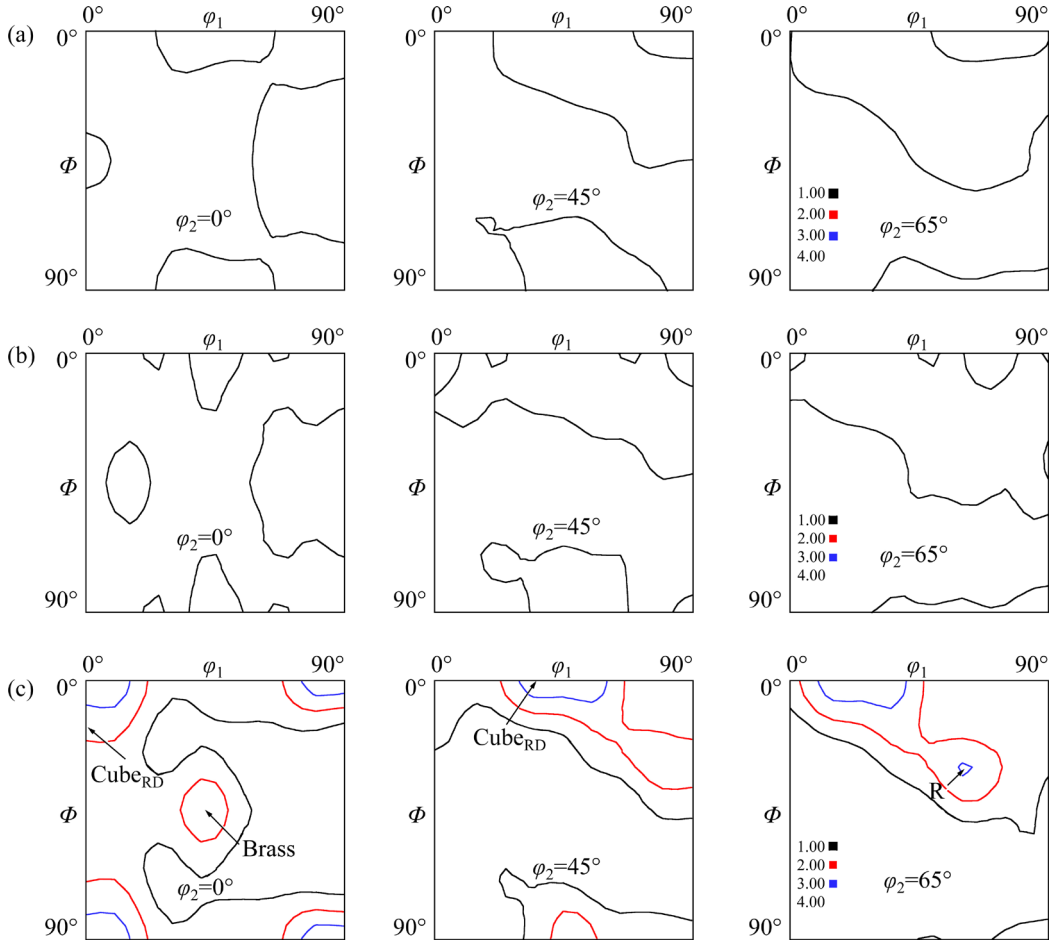

Fig. 12 ODFs of T4P-treated alloy sheets: (a) Sheet A; (b) Sheet B; (c) Sheet C

intensities of 3.16, 3.44 and 2.16, and their volume fractions are 4.86%, 5.93% and 2.82%, respectively. Sheet C still has partial deformation textures of Copper and Brass with orientation intensities of 2.61 and 2.23 and volume fractions of 4.02% and 4.51%, respectively. The results indicate that the hot-rolling deformation has some influence on grain orientation distribution after solution treatment. In summary, it can be found that the differences in the texture of the three cold-rolled sheets are relatively small. Thus, the variance in the number and size of Al(Fe,Mn)Si particles is the primary factor responsible for the differences in the final recrystallization texture. This directly influences the formability of the alloy sheets.

3.3 Formability

The mechanical properties of the T4P-treated alloy sheets are presented in Table 3. The tensile strength, yield strength and elongation of the sheets with different hot-rolling deformation degrees have some differences, and the mechanical properties of the sheets are anisotropic. The tensile strength and elongation of the sheets gradually increase with increasing hot-rolling deformation degree. The yield strength of the sheets shows a decreasing trend with the increase of hot-rolling deformation degree. However, there is little overall change in strength. These small differences in strength are related to grain size and Al(Fe,Mn)Si particle distribution. The differences in the size and number distribution of Al(Fe,Mn)Si particles in the three sheets are significantly different, and these insoluble Al(Fe,Mn)Si particles can contribute significantly to the strength.

Figure 13 summarizes the formability parameters of the T4P-treated alloy sheets. The formability characterized by the average plastic strain ratio (r) and the anisotropy index (Δr) can be expressed as follows [23]:

$$r=(r_0+2r_{45}+r_{90})/4 \quad (2)$$

$$\Delta r=(r_0+r_{90}-2r_{45})/2 \quad (3)$$

where r_0, r_{45} and r_{90} are the r values obtained by tensile testing in the 0°, 45° and 90° directions with respect to the rolling direction, respectively. The strain hardening index (n) is calculated similarly. It can be concluded that as the hot-rolling deformation degree increases, the r value of the sheets increases first and then decreases, while the n value slightly

Table 3 Mechanical properties of T4P-treated alloy sheets

Alloy sheet	Direction/(°)	YS/MPa	UTS/MPa	Elongation/%
A	0	145	257	26.5
	45	148	248	25.5
	90	150	246	26.0
B	0	143	257	29.5
	45	148	253	29.5
	90	141	252	28.5
C	0	143	267	28.0
	45	137	257	30.0
	90	139	257	32.5

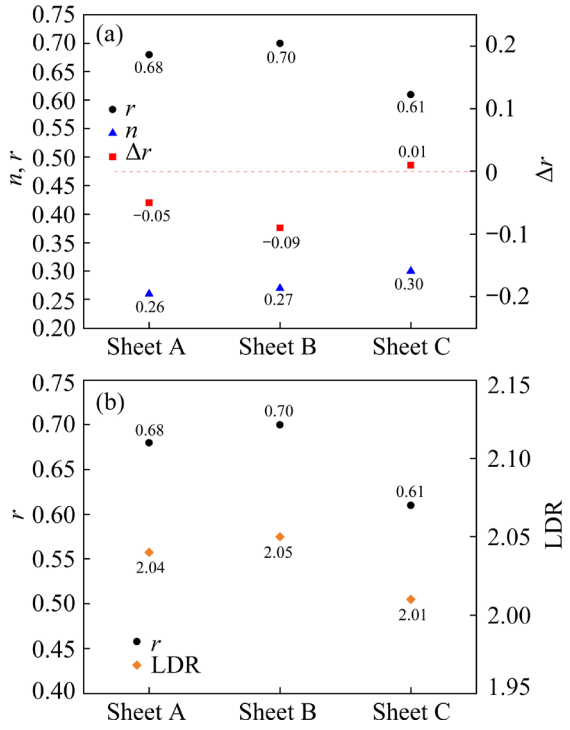

Fig. 13 Formability parameters of T4P-treated alloy sheets (a) and Correlation between r value and LDR value (b)

increases. This suggests that Sheet B possesses the highest formability among the three alloy sheets. Interestingly, the three T4P-treated alloy sheets have smaller Δr values, indicating low planar anisotropy. According to Ref. [5], the calculated results can be more precise when f is set to be 0.9 in Eq. (1). The LDR values of alloy sheets can be determined using Eq. (1) through the utilization of the r and n values. As depicted in Fig. 13(b), the LDR values for Sheets A, B, and C are 2.04, 2.05,

and 2.01, respectively. This represents a positive correlation between the r and LDR values, verifying that Sheet B has the best formability. Based on the mechanical properties results, it can be concluded that the formability of the sheets is influenced by the hot-rolling deformation, which is mainly explained by the formation of different final recrystallization microstructure and textures.

4 Discussion

4.1 Effect of hot-rolling deformation on microstructure

According to the microstructure, the hot-rolling deformation affects the deformation microstructure and the distribution of Al(Fe,Mn)Si, especially in the number and size distribution of Al(Fe,Mn)Si phases. The final recrystallization microstructure and texture largely depend on the deformation microstructure and the second phase. No recrystallization microstructure possibly appears during the hot-rolling process, indicating that the exit temperature of hot-rolling is too low to induce recrystallization or the degree of recrystallization is minimal. The predominance of deformation textures in the hot-rolled sheets suggests that the cooling rate of the whole hot-rolling process is fast, and the deformation degree is low, which is not enough to form more recrystallization textures. Because of the non-uniform deformation, there are some differences in the surface and middle microstructure of the hot-rolled sheet. The deformation of the surface layer is larger, so the grain size is smaller. After cold-rolling, the difference between the middle and surface layers of the sheet is reduced significantly, illustrating that the reduction in the sheet thickness is beneficial to the homogenization of the microstructure. However, there is still a more noticeable variance in Sheet A, which means that a larger deformation is more favorable to homogenizing the microstructure. During the processing, the non-uniformity of deformation is eventually inherited to the T4P-stated sheet, which ultimately affects recrystallization microstructure and texture.

With increasing hot-rolling deformation degree, the number of Al(Fe,Mn)Si particles distributed along the grain boundaries increases, and its size decreases significantly. This reflects that the larger deformation leads to a more broken degree of coarse particles. Different broken degrees of coarse Al(Fe,Mn)Si particles in hot-rolled sheets result in different amounts and size distributions of Al(Fe,Mn)Si particles. After cold-rolling, a typical multi-scale particle distribution characteristic of the coexistence of coarse and fine Al(Fe,Mn)Si can be obtained within the alloy matrix. As shown in Fig. 7, three sheets are distributed with different amounts of Al(Fe,Mn)Si particles in three size ranges, respectively. This difference maintains until the solution treatment, which directly causes differences in recrystallized grain nucleation and growth patterns.

4.2 Effect of Al(Fe,Mn)Si particles on recrystallized grains

The uniformly-diffuse distribution of particles of different sizes within the matrix significantly influences the recrystallization process of cold-rolled sheets. The differences in the particles are mainly reflected in the differences in the number density of multi-scale Al(Fe,Mn)Si particles in this study. From Fig. 7, it can be found that Sheet C has fewer coarse Al(Fe,Mn)Si particles than Sheets A and B, with more micron Al(Fe,Mn)Si particles. Furthermore, there are also many re-solvable submicron Si and Mg_2Si particles in the cold-rolled sheets after the intermediate annealing treatment. Fine particles (<1 μm) inhibit the PSN effect (i.e., the deformation region around the coarse particles provides nucleation sites that stimulate recrystallization nucleation) and delay the formation of $Cube_{ND}$ orientation, while coarse particles (>1 μm) facilitate the formation of $Cube_{ND}$ orientation [24]. The PSN effect provides more nucleation sites around the coarse particles, which promotes recrystallization nucleation, and thus can reduce the recrystallized grain size to some extent. Moreover, the triggering mechanism regarding the PSN effect depends primarily on the number density of particles of different sizes (λ_c), which can be expressed as [25]

$$\lambda_c = \frac{4\gamma_b}{E_D - E_Z} \tag{4}$$

where γ_b, E_D and E_Z are the specific grain boundary energy, the deformation stored energy and the Zener pinning force exerted by the small particle, respectively.

The expression for E_Z is as follows:

$$E_Z=\frac{3F_V\gamma_b}{d_p} \quad (5)$$

where F_V and d_p are the small particle volume fraction and diameter, respectively. The critical grain size parameter that causes the PSN effect increases with raising E_Z, which is heavily affected by the volume fraction and size of the particles.

Combined with the texture analysis (Fig. 12), during the solution treatment, Sheets A and B begin to form grains of weaker $Cube_{ND}$ orientation by the PSN effect, and then grains of other orientations develop gradually with time, as shown in Fig. 14. Due to the larger number of coarse Al(Fe,Mn)Si particles in these two sheets, the non-uniform deformation region occurs near the coarse particles after cold rolling, which increases the dislocation density and produces a large orientation gradient in the vicinity of the particles [26]. This region can be used as a site for PSN nucleation, which promotes the recrystallization nucleation and accelerates the recrystallization. When the grains start to grow out of the deformation zone, the grains are subjected to pinning effect [25], and more fine Al(Fe,Mn)Si particles hinder the grain boundary migration. This makes the growth rate of recrystallized grains in sheet B relatively slower and the average grain size decreases. The combined effect of these two factors eventually leads to a smaller recrystallized grain size in Sheet B according to Figs. 14(e−h). This is also partly attributed to the inheritance of the microstructure during processing due to the larger hot-rolling deformation in the early stage, making the recrystallization microstructure more uniform after solution treatment. Based on the higher number of fine Al(Fe,Mn)Si particles and fewer coarse Al(Fe,Mn)Si particles in Sheet C, the overall size of the second-phase particles in Sheet C is small, and the increase in the dislocation density of the material after cold rolling is limited. Therefore, compared with the other two sheets, the deformation storage energy E_D of Sheet C is lower, and the recrystallization driving force is smaller, which is not conducive to recrystallized nucleation. And due to fewer coarse Al(Fe,Mn)Si particles, the point rotation in the deformation region around the Al(Fe,Mn)Si particles after cold rolling is minor, whereas the PSN nucleation originates from the high strain region around the particles, and the large orientation gradient acts as the site of recrystallization nucleation. As a result, the recrystallized nucleation rate of Sheet C is relatively lower and the size of recrystallized grains after solid solution treatment is larger. Combined with Fig. 12, it is found that the $Cube_{ND}$ texture is predominant in Sheet C, but a small amount of $Cube_{RD}$ orientation is formed by cubic band nucleation. Therefore, it can be inferred that Sheet C is dominated by the nucleation of cubic bands at the initial stage of solution treatment, and the PSN effect is inhibited. The Cube grains grow rapidly

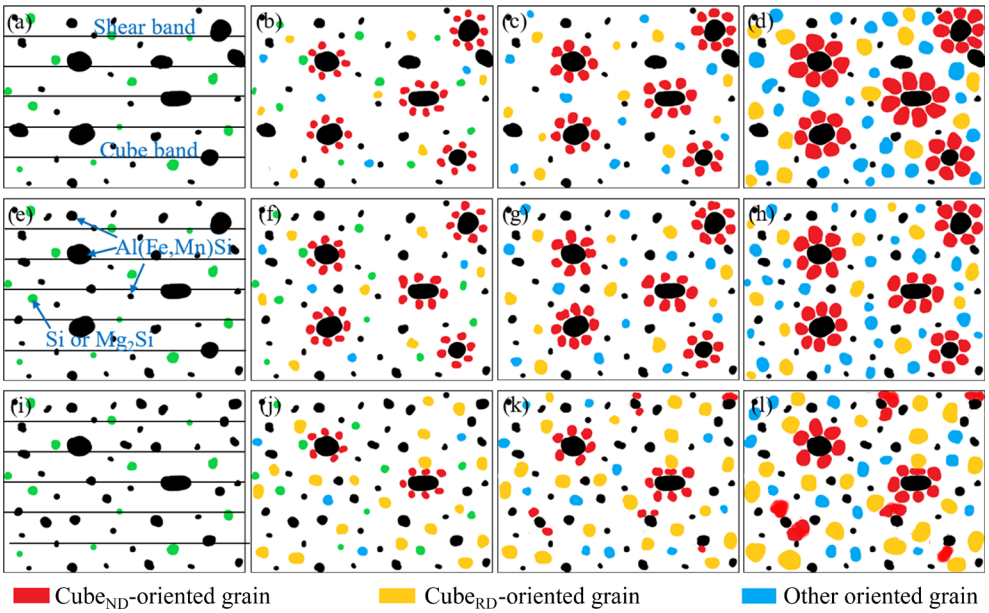

Fig. 14 Schematic illustrations of particle distribution in cold-rolled alloy sheets (a, e, i), process of nucleation and growth of recrystallized grains in Sheets A (c−d), B (f−h) and C (i−l)

during solution treatment. Over time, the Mg_2Si and Si particles gradually dissolve and the grains grow (Figs. 14(i−l)).

4.3 Effect of Al(Fe,Mn)Si particles on recrystallization texture

All textures found in this work after recrystallization belong to well-known $Cube_{ND}$, retaining rolling and random orientations. As the solution time increases, the texture is initially recrystallized from the deformation zone around the particles and in other areas. For Sheets A and B, the $Cube_{ND}$ texture formed by PSN increases as the recrystallized grains grow. When the time is further extended, the grains of other orientations also gradually increase (Fig. 14). It has been studied [27] that the texture intensity first increases slightly as the grain size increases, and then the new texture component replaces the original texture component. Eventually, the orientation intensities of all textures are weak and the textures gradually tend to be randomly distributed, which may be due to slight changes in the grain structure. Since nucleation, mainly controlled by dislocation motion, is less affected by these drag effects than grain boundary motion, the nucleation is reduced. This also verifies that the texture generated by the PSN effect is thoroughly random if the PSN effect reaches a certain level. Because 74% of the hot-rolling deformation leads to more fine particles, the grain growth rate of Sheet B is relatively slow, corresponding to the final recrystallization microstructure observed. To achieve a positive impact from multi-scale particles, it is crucial to ensuring that the number density of both coarse and fine particles in the matrix is well-matched. The decisive step for PSN nucleation is that the size of these particles must exceed the corresponding critical diameter (in Eq. (4)). The larger hot-rolling deformation leads to fewer coarse Al(Fe,Mn)Si particles and more submicron Al(Fe,Mn)Si particles in Sheet C, weakening the PSN effect and allowing the formation of many $Cube_{RD}$ orientations through cube band nucleation at the beginning of solution treatment. With the extension of time, after the gradual dissolution of the particles, the PSN effect gradually dominates and a stronger $Cube_{ND}$ orientation is formed, as shown in Figs. 14(i−l). By contrast, the overly broken fine Al(Fe,Mn)Si particles hinder the PSN effect during the solid solution process and promote grain growth to some extent, reflecting a close relationship between microstructure and texture. It is also possible that due to the inheritance of the texture, more recrystallization texture is present in the cold-rolled Sheet C, causing more recrystallization texture to form even after solution treatment. The R orientation can develop from the rolling texture through discontinuous recrystallization through nucleation from nuclei already existing in the rolling structure [28]. The retained rolling texture is directly from the deformation texture, probably due to the nucleation process at preexisting high-angle boundaries [25].

In summary, the appropriate hot-rolling deformation positively influences randomization of the texture by changing the number density of multi-scale Al(Fe,Mn)Si particles. Therefore, when regulating the hot-rolling deformation of Al−Mg−Si−Zn alloy, the distribution and numbers of Al(Fe,Mn)Si particles need to be precisely controlled to obtain excellent recrystallization microstructure, i.e., reasonable texture distribution and fine grains.

4.4 Effect of recrystallization grain and texture on formability

As reported in a previous study [29], a decrease in the work hardening rate of tensile specimens with higher r values results in a slow onset of diffuse necking, which provides an increased uniform plastic deformation. In addition, a slower reduction in thickness of specimens with higher r values offers good resistance against the onset of failure by localized necking. Thus, a higher r value indicates better formability for metallic polycrystalline materials. It was established that the r value of aluminum alloys is primarily affected by the distribution of texture components and their corresponding volume fractions [11,14]. Additionally, microstructure characteristics such as grain size and morphology also play a role in influencing the r value. Comparing Sheets A and C, Sheet A has a random distribution of grain orientation, while in Sheet C, numerous texture components are present, and none of these textures

is on the γ-fibers. As a result, the r value of Sheet C decreases significantly because the grain morphology and size of these two sheets are identical. The grain orientations of Sheets A and B tend to be randomly distributed, indicating that the textures have almost the same effect. At the same strain, the smaller the average grain size of the sheet, the more difficult it is for the grains to deform in the thickness direction, so the larger the r value of the sheet. Thus, the r value of Sheet A decreases slightly as the grains become noticeably coarser. This also reveals that the r value is more sensitive to the change in texture than grain size.

5 Conclusions

(1) Al(Fe,Mn)Si particles with different size and number distribution characteristics can be obtained by adjusting the hot-rolling deformation. The medium size and number of Al(Fe,Mn)Si particles formed in the sheet at 74% hot-rolling deformation significantly decrease the grain size and improve the uniformity of the microstructure after solution treatment.

(2) The hot-rolled sheets exhibit dissimilar texture characteristics under different hot-rolling deformation degrees. Sheet A is dominated by {013}⟨531⟩ texture, with small amounts of S {123}⟨634⟩ and Copper {112}⟨111⟩ textures. The main texture components of Sheets B and C are Copper, S and Brass {011}⟨211⟩ orientations. During the solid solution treatment, the recrystallization texture evolutions are mainly influenced by the size and number distribution characteristics of Al(Fe,Mn)Si particles modulated by hot-rolling deformation. The grain orientation of the T4P-treated sheets tends to be randomly distributed through 59% and 74% hot-rolling deformation. In comparison, the sheet with 87% hot-rolling deformation has a stronger texture consisting of R {124}⟨211⟩, Cube_{ND} {100}⟨013⟩, Copper and Brass.

(3) The formability of T4P-treated alloy sheets is impacted by grain size and texture; in addition, the texture has a more critical effect on the formability. The medium size and number of Al(Fe,Mn)Si particles formed in the sheet by 74% hot-rolling deformation can refine the grain and weaken the texture, thus increasing the r value and significantly improving the formability of the alloy sheet.

CRediT authorship contribution statement

Kai-xin CHEN: Investigation, Methodology, Writing – Origin draft, Writing − Review & editing; **Li-zhen YAN:** Formal analysis, Writing − Review & editing; **Yong-an ZHANG:** Investigation, Formal analysis, Writing – Review & editing; **Xi-wu LI:** Data curation, Formal analysis; **Zhi-hui LI:** Investigation, Formal analysis; **Hong-wei YAN:** Investigation, Writing − Review & editing; **Lei CHEN:** Resource, Data curation; **Guan-jun GAO:** Supervision, Project administration; **Bai-qing XIONG:** Supervision, Funding acquisition.

Declaration of competing interest

The authors declare that they have no known competing financial interests or personal relationships that could have appeared to influence the work reported in this paper.

Acknowledgments

The authors express their gratitude to the National Key R&D Program of China (Nos. 2020YFF0218200, 2016YFB0300802) for financial support.

References

[1] GRAF A. Materials, design and manufacturing for lightweight vehicles [M]. 2nd ed. Sawston: Woodhead Publishing, 2021.

[2] GHOSH M, GHOSH A, ROY A. Renewable and sustainable materials in automotive industry [J]. Encyclopedia of Renewable and Sustainable Materials, 2020, 3: 162−179.

[3] WANG Bin-ze, ZHANG Zheng-yang, XU Guo-chang, ZENG Xian-lai, HU Wen-tao, MATSUBAE K. Wrought and cast aluminum flows in China in the context of electric vehicle diffusion and automotive lightweighting [J]. Resources, Conservation and Recycling, 2023, 191: 106877.

[4] SINGH P, RAMACHARYULU D A, KUMAR N, SAXENA K K, ELDIN S M. Change in the structure and mechanical properties of Al−Mg−Si alloys caused by the addition of other elements: A comprehensive review [J]. Journal of Materials Research and Technology, 2023, 27: 1764−1796.

[5] SIDOR J, PETROV R H, KESTENS L A I. Deformation, recrystallization and plastic anisotropy of asymmetrically rolled aluminum sheets [J]. Materials Science and Engineering A, 2010, 528: 413−424.

[6] ZHU Shang, LI Zhi-hui, YAN Li-zhen, LI Xi-wu, HUANG Shu-hui, YAN Hong-wei, ZHANG Yong-an, XIONG Bai-qing. Effects of Zn addition on the age hardening

behavior and precipitation evolution of an Al−Mg−Si−Cu alloy [J]. Materials Characterization, 2018, 145: 258−267.

[7] GAO G J, LI Y, WANG Z D, MISRA R D K, DI H S, LI J D, XU G M. Interaction between natural aging and pre-aging processes and its impact on the age-hardening behavior of Al−Mg−Si automotive sheets [J]. JOM, 2019, 71: 4405−4413.

[8] JAIN M, ALLIN J, BULL M J. Deep drawing characteristics of automotive aluminum alloys [J]. Materials Science and Engineering A, 1998, 256: 69−82.

[9] LEU D K. Prediction of the limiting drawing ratio and the maximum drawing load in cup-drawing [J]. International Journal of Machine Tools and Manufacture, 1997, 37: 201−213.

[10] KIM K J, WON S T, PARK J H. Texture analysis of 5182 aluminum alloy sheets for improved drawability by rolling process [J]. Materialwissenschaft und Werkstofftechnik (Materials Science and Engineering Technology), 2012, 43: 373−378.

[11] INOUE H, YAMASAKI T, GOTTSTEIN G, HOUTTE P V, TAKASUGI T. Recrystallization texture and *r*-value of rolled and T4-treated Al−Mg−Si alloy sheets [J]. Materials Science Forum, 2005, 495/496/497: 573−578.

[12] SIDOR J, DECROOS K, PETROV R H, KESTENS L A I. Evolution of recrystallization textures in particle containing Al alloys after various rolling reductions: Experimental study and modeling [J]. International Journal of Plasticity, 2015, 66: 119−137.

[13] WANG Xiao-feng, GUO Ming-xing, PENG Wen-fei, WANG Yong-gang, ZHUANG Lin-zhong. Relationship among solution heating rate, mechanical properties, microstructure and texture of Al−Mg−Si−Cu alloy [J]. Transactions of Nonferrous Metals Society of China, 2021, 31: 36−52.

[14] ZHAO Jing-wei, SHI Xiao-cheng, LIU Meng, LIU Zhen-shan, LU Bing-hui, YU Kang-cai, LI Qing, RAN Ji-long, ZHAO Pi-zhi. Effect of hot rolling finishing temperature and intermediate annealing on the micro-structure, texture evolution, and comprehensive properties of Al−Mg−Si alloy [J]. Journal of Alloys and Compounds, 2024, 970: 172525.

[15] LI Jia-chen, WU Xiao-dong, CAO Ling-fei, LIAO Bin, WANG Yi-chang, LIU Qing. Hot deformation and dynamic recrystallization in Al−Mg−Si alloy [J]. Materials Characterization, 2021, 173: 110976.

[16] LI Hui, WANG Jia-yi, YAN Shao-hui, MI Zhen-li, JIANG Hai-tao. Evolution of microstructure and texture gradients in the thickness direction of isothermal hot-rolled Al−Mg−Si alloys [J]. Chinese Journal of Rare Metals, 2019, 43: 265−273. (in Chinese)

[17] CHEN Kai-xin, YAN Ll-zhen, ZHANG Yong-an, LI Xi-wu, LI Zhi-hui, GAO Guang-jun, LIU Hong-wei, XIONG Bai-qing. Microstructure, texture and formability control by initial hot-rolling temperature of Al−Mg−Si Alloy [J]. Advanced Engineering Materials, 2022, 24: 2101705.

[18] WANG Xiao-feng, GUO Ming-xing, ZHANG Ji-shan, ZHUANG Lin-zhong. Effect of Zn addition on the microstructure, texture evolution and mechanical properties of Al−Mg−Si−Cu alloys [J]. Materials Science and Engineering A, 2016, 677: 522−533.

[19] WANG Xiao-feng, GUO Ming-xing, LUO Jin-ru, ZHU Jie, ZHANG Ji-shan, ZHUANG Lin-zhong. Effect of Zn on microstructure, texture and mechanical properties of Al−Mg−Si−Cu alloys with a medium number of Fe-rich phase particle [J]. Materials Characterization, 2017, 134: 123−133.

[20] YU Li-bo, CHEN Lin, WANG He-bin, WANG Xiong-feng, PENG Wen-fei, WANG Yong-gang, ZHUANG Lin-zhong. Influence of Fe-rich particles on microstructure evolution, texture and mechanical properties of Al−Mg−Si−Cu alloys [J]. Metallurgical Research and Technology, 2020, 117: 508.

[21] YANG H W, WIDIANTARA I P, KO Y G. Effect of deformation path on texture and tension properties of submicrocrystalline Al−Mg−Si alloy fabricated by differential speed rolling [J]. Materials Letters, 2018, 213: 54−57.

[22] LI Xin-yu, XIA Wei-ju, CHEN Ji-hua, YAN Hong-ge, LI Zhen-zhen, SU Bin, SONG Min. Dynamic recrystallization, texture and mechanical properties of high Mg content Al−Mg alloy deformed by high strain rate rolling [J]. Transactions of Nonferrous Metals Society of China, 2021, 31: 2885−2898.

[23] LÜCKE K, ENGLER O. Effects of particles on development of microstructure and texture during rolling and recrystallisation in fcc alloys [J]. Materials Science and Technology, 1990, 6: 1113−1130.

[24] ENGLER O, HIRSCH J. Recrystallization textures and plastic anisotropy in Al−Mg−Si sheet alloys [J]. Materials Science Forum, 1996, 217−222: 479−486.

[25] VATNE H E, ENGLER O, NES E. The effect of precipitates on texture development [J]. Materials Science Forum, 1994, 157−162: 1501−1506.

[26] CHEN Kai-xin, YAN Li-zhen, ZHANG Yong-an, LI Xi-wu, LI Zhi-hui, GAO Guan-jun, YAN Hong-wei, XIONG Bai-qing. Enhanced formability of Al−Mg−Si−Zn alloy sheet via dislocation structure and texture during cold rolling [J]. Journal of Materials Research and Technology, 2024, 28: 3306−3318.

[27] WANG Xiao-feng, SHI Tong-ya, JIANG Zhao-xiu, CHEN Wei, GUO Ming-xing, ZHANG Ji-shan, ZHUANG Lin-zhong, WANG Yong-gang. Relationship among grain size, texture and mechanical properties of aluminums with different particle distributions [J]. Materials Science and Engineering A, 2019, 753: 122−134.

[28] ENGLER O. On the origin of the R orientation in the recrystallization textures of aluminum alloys [J]. Metallurgical and Materials Transactions A, 1999, 30: 1517−1527.

[29] OH G J, LEE K M, HUH M Y, PARK J E, PARK S H, ENGLER O. Effect of *r*-value and texture on plastic deformation and necking behavior in interstitial-free steel sheets [J]. Metals and Materials International, 2017, 23: 26−34.

热轧变形对 Al−Mg−Si−Zn 合金板材的晶粒、织构及成形性能的影响

陈凯欣[1,2,3]，闫丽珍[1,2,3]，张永安[1,2,3]，李锡武[1,2,3]，
李志辉[1,3]，闫宏伟[1,2,3]，陈 雷[4]，高冠军[1,2]，熊柏青[1,3]

1. 中国有研科技集团有限公司 有色金属材料制备加工国家重点实验室，北京 100088；
2. 有研工程技术研究院有限公司，北京 101407；
3. 北京有色金属研究总院，北京 100088；
4. 东北轻合金有限责任公司，哈尔滨 150060

摘 要：采用光学显微镜(OM)、扫描电子显微镜(SEM)、透射电子显微镜(TEM)、X 射线衍射仪(XRD)和拉伸试验，系统研究了不同热轧变形量对 Al−Mg−Si−Zn 合金的显微组织演变、织构演变和成形性能的影响。结果表明，通过调整热轧变形量(59%、74%和 87%)可以获得不同尺寸和数量分布的 Al(Fe,Mn)Si 颗粒，这些颗粒分布的差异是影响固溶处理过程中再结晶形核和晶粒生长的主要因素。T4P 处理后，热轧变形量为 59%和 74%的 Al−Mg−Si−Zn 合金板材中晶粒取向趋于随机分布，而热轧变形量为 87%的板材中存在 R{124}⟨211⟩、$Cube_{ND}${100}⟨013⟩、Copper{112}⟨111⟩和 Brass{011}⟨211⟩织构。热轧变形量为 74%时获得的中等尺寸和数量的 Al(Fe,Mn)Si 颗粒在固溶处理后使板材中形成细小的晶粒和随机分布的织构，明显提高 Al−Mg−Si−Zn 合金的成形性能。

关键词：Al−Mg−Si−Zn 合金；热轧变形；Al(Fe,Mn)Si 颗粒；晶粒；织构；成形性能

(Edited by Bing YANG)